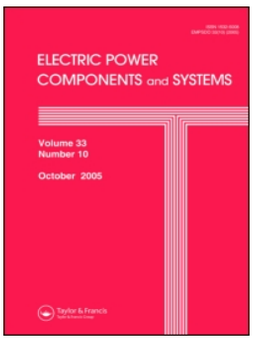

Taylor & Francis
Taylor & Francis Group

Electric Power Components and Systems

ISSN: 1532-5008 (Print) 1532-5016 (Online) Journal homepage: http://www.tandfonline.com/loi/uemp20

Offshore Wind Energy System with DC Transmission Discrete Mass: Modeling and Simulation

Mafalda Seixas, Rui Melício & Victor Mendes

To cite this article: Mafalda Seixas, Rui Melício & Victor Mendes (2016) Offshore Wind Energy System with DC Transmission Discrete Mass: Modeling and Simulation, Electric Power Components and Systems, 44:20, 2271-2284, DOI: 10.1080/15325008.2016.1219887

To link to this article: http://dx.doi.org/10.1080/15325008.2016.1219887

Published online: 28 Nov 2016.

Electric Power Components and Systems, 44(20):2271–2284, 2016

ISSN: 1532-5008 print / 1532-5016 online
DOI: 10.1080/15325008.2016.1219887

Taylor & Francis
Taylor & Francis Group

Offshore Wind Energy System with DC Transmission Discrete Mass: Modeling and Simulation

Mafalda Seixas,[1,2,3] Rui Melício,[1,2] and Victor Mendes[2,3]
[1]IDMEC/LAETA, Instituto Superior Técnico, Universidade de Lisboa, Lisbon, Portugal
[2]Departamento de Física, Escola de Ciências e Tecnologia, Universidade de Évora, Évora, Portugal
[3]Department of Electrical Engineering and Automation, Instituto Superior de Engenharia de Lisboa, Lisbon, Portugal

CONTENTS

Abstract—This article presents an integrated model for an offshore wind energy system taking into consideration a contribution for the marine wave and wind speed with perturbations influences on the power quality of current injected into the electric grid. The article deals with the simulation of one floating offshore wind turbine equipped with a permanent magnet synchronous generator and a two-level converter connected to an onshore electric grid. The use of discrete mass modeling is accessed in order to reveal by computing the total harmonic distortion on how the perturbations of the captured energy are attenuated at the electric grid injection point. Two torque actions are considered for the three-mass modeling, the aerodynamic on the flexible part and on the rigid part of the blades. Also, a torque due to the influence of marine waves in deep water is considered. Proportional integral fractional-order control supports the control strategy. A comparison between the drive train models is presented.

Keywords: offshore wind turbine system, discrete mass modeling, DC link, power converter, simulation
Received 21 June 2015; accepted 23 July 2016
Address correspondence to Rui Melício, IDMEC/LAETA, Instituto Superior Técnico, Universidade de Lisboa, Av. Rovisco Pais 1, 1049-001 Lisbon, Portugal. E-mail: ruimelicio@gmail.com
Color versions of one or more of the figures in the article can be found online at www.tandfonline.com/uemp.

1. INTRODUCTION

The global energy demand in 2040 is expected to be about 30% higher than that of 2010 [1], therefore, it can be predicted that more challenges such as increased environmental problems, depletion of fossil fuels, and unstable oil prices will intensify [2]. The majority of the energy used by the society comes from the use of conventional fossil fuels, but the use of fossil fuels accounts for 80% of anthropogenic gas emission [3]. The use of renewable energy sources is crucial in order to decarbonize the energy industry [4], and in recent years there has been a rapid increase in power capacity and energy conversion from these sources, mostly regarding the use of wind energy. Although, onshore wind energy conversion is less expensive than offshore, for instance, the costs of operation and maintenance for offshore wind energy conversion are approximately 2–4 times to that of the onshore [5], finding new suitable available onshore sites is becoming difficult, especially in Europe [6]. Particularly, developments in offshore wind power were achieved with the research and exploitation on floating wind

NOMENCLATURE

v = Perturbed wind speed
v_0 = Average wind speed
n = Kind of the mechanical eigenswing excited by the rotation movement
A_n = Magnitude of the eigenswing n
ω_n = Eigenfrequency of the n eigenswing
P_b = Mechanical power of the wind turbine with dynamic perturbations
P_{bb} = Mechanical power captured by the wind turbine without dynamic perturbations
ρ = Air density
R = Radius of the area cover by the blades, OB part
c_p = Power coefficient
ζ = Pitch angle of the turbine blades
λ_R = Tip speed ratio, at radius R
λ_r = Local speed ratio, at radius r
r = Radius of the rigid part of the blades, OA part
m = Order of the harmonic of an eigenswing
a_{nm} = Normalized magnitude of g_{nm}
g_{nm} = Distribution of the m-order harmonic in the n eigenswing
h_n = Modulation of the n eigenswing
φ_{nm} = Phase of the m-order harmonic in the n eigenswing
η = Wave elevation for x, y position as a function of time
η_a = Vector of harmonic wave amplitudes
ϑ = Vector of harmonic wave frequencies
ε = Vector of harmonic wave phases (random)
ϕ = Vector of harmonic wave numbers
ψ = Vector of harmonic wave directions
M_{mb} = One and two-mass, wind turbine mechanical torque
M_{mfb} = Three-mass, wind turbine flexible blade part mechanical torque
M_{mrb} = Three-mass, wind turbine rigid part of the blades mechanical torque
M_{stp} = All mass models, tower and platform stiffness torque due to floating surface motion
M_{rb} = Two-mass, turbine bearing resistant torque
M_{rah} = Two-mass, hub and blades viscosity airflow resistant torque
M_{sb} = Two-mass, shaft stiffness torsional torque
M_{re} = Two and three-mass, generator bearing resistant torque
M_{rae} = Two-mass, generator viscosity airflow resistant torque
M_e = All mass models, electric torque
M_{rfb} = Three-mass, flexible blades part bearing resistant torque
M_{sfbh} = Three-mass, shaft stiffness torque between flexible blades part and hub
M_{rh} = Three-mass, hub bearing resistant torque
M_{she} = Three-mass, shaft stiffness torque between hub and generator
ω_w = Marine wave frequency
ω_b = One- and two-mass, angular speed of the turbine.
ω_e = All mass models, angular speed of the generator
ω_{fb} = Three-mass, angular speed of the flexible blades
ω_{rbh} = Three-mass, angular speed of the rigid part of the blades plus hub
k_{stp} = All mass models, stiffness elastic coefficient due to floating surface motion
k_{sb} = Two-mass, shaft stiffness elastic coefficient
k_{sfbh} = Three-mass, shaft stiffness elastic coefficient between flexible blades and hub
k_{she} = Three-mass, shaft stiffness elastic coefficient between hub and generator
J = One-mass, moment of inertia for blades, hub, tower, platform, and generator
J_b = Two-mass, blades, hub, tower, and platform moment of inertia
J_e = Two- and three-mass, generator moment of inertia
J_{fb} = Three-mass, flexible blades part moment of inertia
J_{rbh} = Three-mass, rigid blades part plus hub, tower, and platform moment of inertia
i_{sd}, i_{sq} = Stator dq currents
L_{sd}, L_{sq} = Stator dq inductances
R_{sd}, R_{sq} = Stator dq resistances
u_{sd}, u_{sq} = Stator dq voltages
p = Number of pairs of poles
L_m = Mutual inductance
i_{er} = Equivalent rotor current.
u_{er} = Equivalent rotor voltage
i_{gy} = Electric grid injected current
P_e = Electric power
L_g,R_g = Electric grid inductance and resistance
u_{gy} = Filter voltage
u_y = Electric grid voltage
u_{sy} = Converter voltage
i_y = Converter current
u^*_{dc} = Reference voltage
u_{dc1} = Capacity bank C_1 voltage, i.e., continuous rectifier output voltage
u_{dc2} = Capacity bank C_2 voltage, i.e., inverter input voltage
L_{dc}, R_{dc} = Submarine cable inductance and resistance
C_{dc} = Submarine cable capacity
i_{dc} = Submarine cable current

turbines [7], taking advantage of vast areas of available sea and of favorable wind conditions which are reported as tending to be considerably better and less variable than onshore ones [8].

Offshore structures are influenced by marine wind and wave dynamics. For instance, the authors in [9] consider the influence of the floating support structure motion on the strength of the blades and shaft, and the force induced by the combined rotational, translational and angular motion of the blades due to the coupling effects of the dynamics. Hence, there is a need to access how important are the loads in disturbing the conversion in what regards electric energy quality.

Offshore deployment for conversion of wind energy allows the use of higher rotor dimension due to less restrictions of scale which enables the use of larger turbines. This fact leads to a need for a proper design of the drive train of the wind energy system besides higher requirement of turbine reliability [10]. That being said, the model for an offshore wind energy system (OWES) has to take into account the flexibility of the mechanical structure, due to the height and the tendency to oscillate [11] and will be highly non-linear. Oversimplification on the modeling of the OWES could introduce significant error in the value of the results.

As wind energy is increasingly integrated into power systems, electric energy quality is becoming an important concern and presents many challenges to modern power systems [12]. One of the indices that measures the electric energy quality is the total harmonic distortion (THD). The standard IEEE-519 imposes a maximum limit of 5% for the electrical current THD. While the application of the standard IEEE-519 is not mandatory for OWES this THD value is followed as a guideline for evaluation purposes.

Variable speed operation technology based on the use of permanent magnet synchronous generator (PMSG) as an alternative to conventional synchronous generators as the advantages generally stated for wind power applications: the higher efficiency, due to null copper losses in the rotor [13]; the exclusion of the gearbox, due to ability to operate at low speed [14]. A variable speed wind turbine equipped with a PMSG needs an electronic full-power converter in order to convert the energy captured from the wind into electric energy at a non-constant frequency into constant one. The type of power transmission technology in offshore depends on the distance between the floating platforms and the grid connection point. For shorter distances, below 50 km, alternated current (AC) can be used, but for longer distances direct current (DC) becomes the most suitable solution [15]. DC transmission technology presents advantages such as low power losses, no connection distance limitation, and no resonance. But, also present disadvantages regarding control and switching actions. However, transmission distances limitation causes high voltage direct current (HVDC) transmission technology to be a better option. Consequently, submarine cables and DC circuit breakers (CBs) are important components of HVDC transmission technology [16]. HVDC light appeared as a power transmission technology particularly suitable for medium- to small-scale power transmission applications [17, 18]. Actually, the number of submarine cable links being installed worldwide is rapidly increasing. Submarine cable technology has advanced to allow the manufacture of cables for bulk power transfer between transmission systems in lengths up to 100 km [19].

This article presents a model for a simulation of a OWES with a wind power as the one named WindFloat, located at Aguçadoura, Portugal at 5 km of shore, but considering a 5 kV HVDC light transmission link, similar to the Helljsön project, Sweden at 10 km between bars with ± 10 kV [20]. The model considers an offshore variable-speed turbine with a power output of 2 MW in deep water equipped with a PMSG using full-power two-level converter (TLC). Also, a submarine cable is considered to guide electrical energy through a DC link from the variable frequency source to the injected energy into the electric grid with constant frequency. The wind turbine part of the system rests on a tri-column triangular floating platform partially submerged with the wind turbine located on top of one of the columns, and the other two columns have more ballast to stabilize the entire platform. The platform is moored using a conventional catenary mooring system [21] linking the floating platform to structures made of concrete, which are in turn anchored to the marine soil.

The mechanical drive train, the structure and the moving floating surface dynamics is considered by three approaches, respectively, one-mass, two-mass, or three-mass, in order to discuss which are more appropriated in detaining the THD. The three-mass model is considered in order to isolate the aerodynamics influence on the flexible part of the blades from the rigid one. This isolation is associated with the two mechanical torques acting on the respective parts of the blades. The controllers used in the converters are fractional-order proportional integral (PI^{μ}) ones. Also, pulse width modulation (PWM) by space vector modulation (SVM) associated with sliding mode (SM) is used for controlling the converters.

The configuration considered in this article for the OWES with TLC is shown in Figure 1.

However, when considering more than one wind turbine, i.e., more than one generation unit, there is not one particular configuration, depending on the capacity of the offshore wind farm groups of turbines are possible to be considered, but regarding not only the economy on the design, but also fallibility on the operation.

Advance technology and better control systems for wind turbines operation connected with electric grid allow some flexibility on the requirements for the performance of electric generators. One of the most severe requirements in the

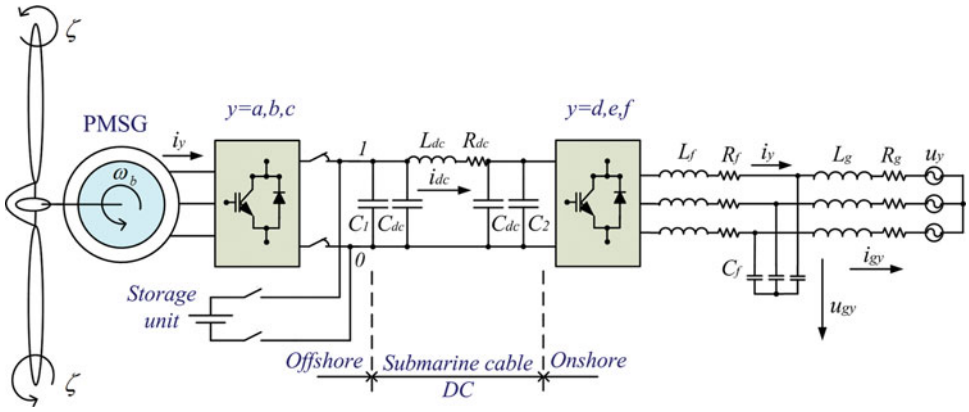

FIGURE 1. OWES with TLC and submarine cable.

case of offshore wind farms could be the black-start capability which requires the ability to recover from a total or partial shutdown within a timeframe without any external supply [16, 22].

In case of sudden disconnection, an auxiliary service, such as a battery storage unit, may be connected at the end of the rectifier, Figure 1, in order to maintain system reliability and supply continuity to the capacitors banks achieving a successful black-start [23].

The rest of the article is organized as followed: Section 2 presents the mechanical modeling, taking into consideration the dynamics associated with the action excited by wind and marine wave on all physical structure on a one-, a two-, or a three-mass modeling for the rotor of the wind turbine and generator. Section 3 presents the electric modeling, taking into consideration the TLC, the submarine cable, the second order filter, and the electric grid. Section 4 presents the fractional calculus theory. Section 5 presents the control modeling: PWM by SVM associated with SM for controlling the converter. Section 6 presents the case studies and the simulation results, using Matlab (The MathWorks, Natick, Massachusetts, USA)/Simulink language. Section 7 presents the concluding remarks.

2. MECHANICAL MODELING

The wind speed has a model consisting in a finite sum of harmonic terms with frequencies range in 0.1–10 Hz, given by:

$$v = v_0 \left[1 + \sum_n A_n \, \sin(\omega_n \, t) \right] \tag{1}$$

The mechanical power of the wind turbine has a model taking into consideration three perturbations of the dynamics associated with the action excited by the wind on all physical structure [24]. The mechanical power is given by:

$$P_b = P_{bb} \left[1 + \sum_{n=1}^{3} I_n(t) \right] \tag{2}$$

where

$$P_{bb} = \frac{1}{2} \rho \, \pi \, R^2 \, v^3 c_p \tag{3}$$

The power coefficient c_p is a function of the tip speed ratio λ_R and of the pitch angle ζ. The determination of this coefficient requires the use of blade element theory and the knowledge of blade geometry. Normally, numerical approximations are advised as for instance the one developed in [25] followed in this article.

The mechanical power in Eq. (2) is computed by a multiplicative term in Eq. (3) given by the well-known formula for the mechanical power captured by the wind turbine without dynamic perturbations [24]. There are three perturbations considered, respectively: I_1 the asymmetry in the turbine, I_2 the vortex tower interaction, and I_3 the eigenswings in the blades. Both perturbations are modeled by a sum [24] given by:

$$I_n(t) \; = A_n \left(\sum_{m=1}^{2} a_{nm} \; g_{nm}(t) \right) \; h_n(t) \tag{4}$$

where

$$g_{nm}(t) = \sin \left(\int_0^t m \; \omega_n(t') \, dt' \; + \; \varphi_{nm} \right) \tag{5}$$

The dynamics associated with the asymmetry in the turbine is assessed considering the following data: $A_1 = 0.01, a_{11} = 4/5, a_{12} = 1/5, \; \omega_1(t) = \omega_t(t), \; \varphi_{11} = 0, \; \varphi_{12} = \pi/2.$

The dynamics associated with the vortex tower interaction is assessed considering the following data: $A_2 = 0.08, a_{21} = 1/2, a_{22} = 1/2, \; \omega_2(t) = 3\,\omega_t(t), \; \varphi_{21} = 0, \; \varphi_{22} = \pi/2.$

The dynamics associated with the eigenswings in the blades is assessed considering the following data: $A_3 = 0.15, a_{31} = 1,\ \omega_2(t) = 1/2\ [g_{11}(t) + g_{21}(t)],\ \varphi_{31} = 0$.

The marine wave model [26] for all the drive train models is given by:

$$\eta(x, y, t) = \sum_{i=1}^{n} \eta_a(i) \cos[\vartheta(i)t + \varepsilon(i) - \phi(i)(x \cos(\psi(i)) + y \sin(\psi(i))] \quad (6)$$

The elastic behavior of the tower and platform due to the influence of marine waves, in deep water, for all the drive train models causes a resistant torque [27] given by:

$$M_{stp} = k_{stp}\ \omega_w \quad (7)$$

The behavior of the mechanical drive train of an OWES has a model consisting in a set of discrete inertia masses connected together by springs and dampers. The one-mass drive train model considers all inertia components lumped together, i.e., modeled as a single rotating mass.

The mechanical torque of the wind turbine subject to a wind without perturbations, in the case of the drive train described by a shaft with one or two-mass model, considering Eq. (3) is given by:

$$M_{mb} = \frac{1}{2} \frac{\rho\, \pi\, R^5 \omega_b^2}{\lambda_R^3} c_p \quad (8)$$

The equation for the one-mass model is based on the second law of Newton, deriving the state equation for the rotor angular speed at the wind turbine, given by:

$$\frac{d\omega_b}{dt} = \frac{1}{J} (M_{mb} + M_{stp} - M_e) \quad (9)$$

The drive train configured by two-mass model has a first mass to concentrate inertia of the blades, hub, tower, and platform; a second mass to concentrate the generator inertia. This configuration is shown in Figure 2.

The equations for the two-mass model are based on the torsional version of the second law of Newton, deriving the state equation for the rotor angular speed at the wind turbine and for the rotor angular speed at the generator, given by:

$$\frac{d\omega_b}{dt} = \frac{1}{J_b} (M_{mb} + M_{stp} - M_{rb} - M_{rah} - M_{sb}) \quad (10)$$

$$\frac{d\omega_e}{dt} = \frac{1}{J_e} (M_{sb} - M_{re} - M_{rae} - M_e) \quad (11)$$

The increase in size of the wind turbines implies that the blades are more flexible and tend to bend. Since the blade bending occurs at a significant distance from the joint between the blades and the hub is admissible to model the blades by splitting them in two parts. The blade bending dynamics is explained by a torsional system as shown in Figure 3.

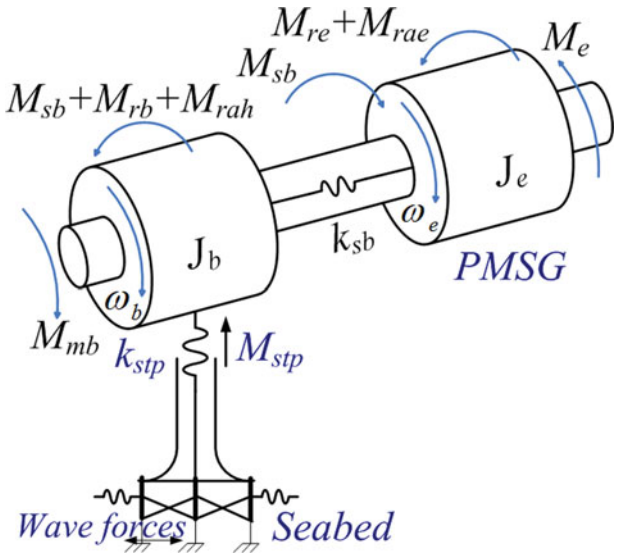

FIGURE 2. Two-mass drive train model.

The first part, OA, is defined from the blade root to a point of radius r of the wingspan with a rigid behavior; the second part, AB, is defined from the point of radius r to the edge of the blade with a flexible behavior. The rigid part of the blades is formed by sectors OA1, OA2, and OA3 and the flexible part of the blades is formed by sectors A1B1, A2B2, and A3B3.

One of the aeroelastic problems for large wind turbines is due to the fact that the lead-lag and flap frequencies of the blades may come closer together during the up-scaling of the turbines. This, in combination with stalled flow can result in aeroelastic instabilities [28]. The damage resulted from severe aeroelastic instabilities producing longitudinal cracks on the flexible part of the blade near the root. The lead-lag and flap aeroelastic stability of wind turbine blade sections is simulate as a model resulting from the combination of a spring-mass-damper-equivalent structural model [29]. The drive train configured by three masses has a first mass to concentrate the

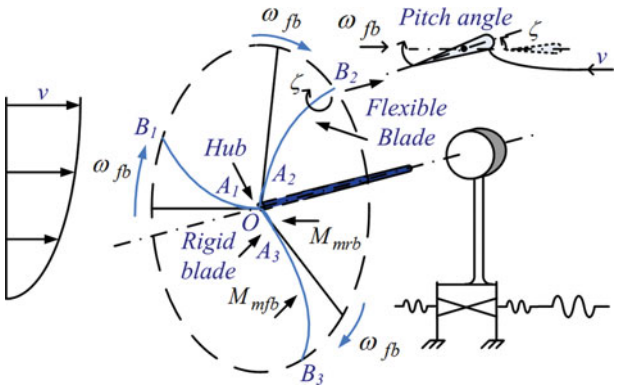

FIGURE 3. Blade bending dynamic system.

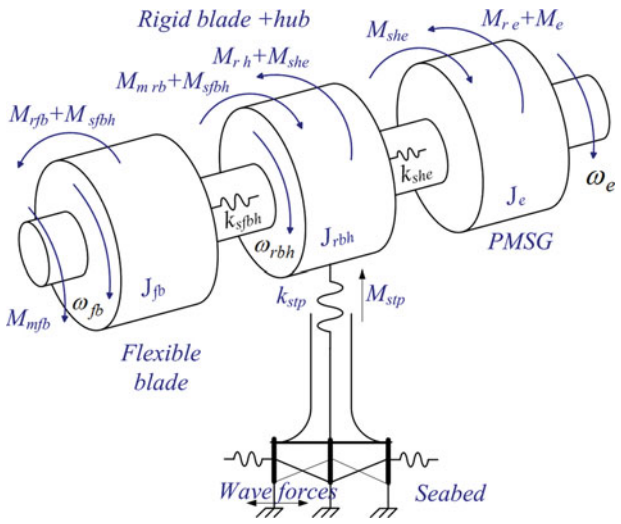

FIGURE 4. Three-mass drive train model.

inertia of the flexible part of the blades; a second mass to concentrate the rigid part of the blades, hub, tower, and platform; a third mass to concentrate the inertia of the generator similar to the second mass of the two-mass model. The connection between the three masses is made through elastic couplings [30]. The three-mass model is shown in Figure 4.

The modeling analysis uses the following assumptions: (1) the wind speed v is the same across the blade radius; (2) the blade span has a modeling consisting in an association of two different blade parts, a rigid and a flexible; (3) the blade angular speed in flexible and rigid part is almost the same and have very small fluctuations over the average angular speed; (4) the power coefficient c_p for both parts as a function of the respective speed ratios has the same value. Assume a radius r of 2.5 m for the rigid part of the blades, as shown in Figure 5.

The tip speed ratio λ_R, is defined as the ratio of the blade tip speed to the wind speed is given by:

$$\lambda_R = \frac{\omega_{fb} R}{v} \tag{12}$$

The local speed ratio λ_r, is defined as the ratio of the rotor speed at some intermediate radius to the wind speed [31] is given by:

$$\lambda_r = \frac{\omega_{rbh} r}{v} \tag{13}$$

The mechanical power for the blade flexible part is given by:

$$\mathrm{P}_{fb} = \frac{1}{2}\rho\,\pi\,(R^2 - r^2)\,v^3 c_p \tag{14}$$

The mechanical power for the rigid part of the blades is given by:

$$\mathrm{P}_{rb} = \frac{1}{2}\rho\,\pi\,r^2\,v^3 c_p \tag{15}$$

The mechanical torque of the flexible part of the blades subject to a wind without perturbations, in the case of the drive train described by a shaft with three masses, considering Eq. (12) and Eq. (14), is given by:

$$M_{mfb} = \frac{1}{2}\frac{\rho\,\pi\,(R^2 - r^2)\omega_{fb}^2 R^3}{\lambda_R^3} c_p \tag{16}$$

The mechanical torque of the rigid part of the blades subject to a wind without perturbations, in the case of the drive train described by a shaft with three masses, considering Eq. (13) and Eq. (15), is given by:

$$M_{mrb} = \frac{1}{2}\frac{\rho\,\pi\,r^5\omega_{rbh}^2}{\lambda_r^3}\,c_p \tag{17}$$

The equations for the three-mass model are based on the torsional version of the second law of Newton, deriving the state equations for the rotor angular speed at the flexible blade part, the rotor angular speed at the rigid part of the blades plus hub of the wind turbine and for the rotor angular speed at the generator, given by:

$$\frac{d\omega_{fb}}{dt} = \frac{1}{J_{fb}}(M_{mfb} - M_{rfb} - M_{sfbh}) \tag{18}$$

$$\frac{d\omega_h}{dt} = \frac{1}{J_{rbh}}(M_{sfbh} + M_{mrb} + M_{stp} - M_{rh} - M_{she}) \tag{19}$$

$$\frac{d\omega_e}{dt} = \frac{1}{J_e}(M_{she} - M_{re} - M_e) \tag{20}$$

3. ELECTRIC MODELING

The equations for modeling a PMSG are shown in [12] and are given by:

$$\frac{di_{sd}}{dt} = \frac{1}{L_{sd}}(u_{sd} + p\omega_e L_{sq}\, i_{sq} - R_{sd}\, i_{sd}) \tag{21}$$

$$\frac{di_{sq}}{dt} = \frac{1}{L_{sq}}[u_{sq} - p\omega_e(L_{sd}\, i_{sd} + L_m\, i_{er}) - R_{sq}\, i_{sq}] \tag{22}$$

with the electric power given by:

$$P_e = [\,u_{sd}\;u_{sq}\;u_{er}\,]\,[\,i_{sd}\;i_{sq}\;i_{er}\,]^T \tag{23}$$

But in Eq. (23), due to the consideration of avowing demagnetization of the permanent magnet in the PMSG [32], a null reference stator direct component current $i_{sd}^* = 0$ has to be imposed.

The AC-DC-AC TLC is implemented with 12 unidirectional commanded insulated gate bipolar transistors in order to implement the rectifier and the inverter functionality [12]. The configuration considered in this paper for the OWES with TLC is shown in Figure 1.

The TLC is an AC-DC-AC converter, having six transistors identified by S_{ik}, used as a rectifier and with six similar transis-

tors used as an inverter. The rectifier is connected between the PMSG and a capacitor bank. The inverter is connected between this capacitor bank and a second order filter, which in turn is connected to an electric grid. The grouping of two transistors connected to the same phase constitutes the arm y of the converter. The switching variable γ_y is used to identify the state of the transistor h in the leg y of the TLC ascertain the switching function of each transistor. The index h with $h \in \{a,\ b\}$ recognize the transistor. The index y with $y \in \{a,\ b, c\}$ recognizes the arms for the rectifier and $y \in \{d, e,\ f\}$ recognizes the arms for the inverter. The valid constrains [33, 34] for the γ_y of each arm y are given by:

$$\gamma_y = \begin{cases} 1, & (S_{ay} = 1 \ and \ S_{by} = 0) \\ 0, & (S_{by} = 1 \ and \ S_{ay} = 0) \end{cases} \quad y \in \{a,\ \dots,\ f\} \tag{24}$$

The rectifier input voltage is given by:

$$u_{sy} = \frac{1}{3}\left(2\gamma_y - \sum_{\substack{j=a \\ j\neq y}}^{c} \gamma_j\right) u_{dc1} \quad y \in \{a,\ b, c\} \tag{25}$$

The state equation of the DC voltage at the capacity bank C_1 terminals is given by:

$$\frac{du_{dc1}}{dt} = \frac{1}{C_1 + C_{dc}}\left(\sum_{y=a}^{c} \gamma_y i_y - i_{dc}\right) \tag{26}$$

The impedance of the submarine cable is represented by a π equivalent electric circuit model, for the medium line modeling is used [18]. The current in the submarine cable is given by:

$$\frac{di_{dc}}{dt} = \frac{1}{L_{dc}}(u_{dc1} - u_{dc2} - R_{dc}\, i_{dc}) \tag{27}$$

The state equation of the DC voltage at the capacity bank C_2 terminals is given by:

$$\frac{du_{dc2}}{dt} = \frac{1}{C_2 + C_{dc}}\left(i_{dc} - \sum_{y=d}^{f} \gamma_y i_y\right) \tag{28}$$

The inverter output voltage is given by:

$$u_{sy} = \frac{1}{3}(2\gamma_y - \sum_{\substack{j=d \\ j\neq y}}^{f} \gamma_j)\, u_{dc2} \quad y \in \{d, e,\ f\} \tag{29}$$

The second order filter is given by:

$$\frac{du_{gy}}{dt} = \frac{1}{C_f}(i_y - i_{gy}) \quad y \in \{d, e,\ f\} \tag{30}$$

The electric grid has a model consisting in an equivalent three-phase active symmetrical circuit with a series of a resistance and an inductance. Hence, for electric current injected into the electric grid, see Figure 1, the state equation is given by:

$$\frac{di_{gy}}{dt} = \frac{1}{L_g}(u_{gy} - R_g i_{gy} - u_y) \quad y \in \{d, e,\ f\} \tag{31}$$

4. FRACTIONAL CALCULUS

Fractional-order controller strategy is supported by the theory of Fractional calculus. Fractional calculus generalizes ordinary differentiation and integration calculus and it can be seen as the extension of it to include an arbitrary, non-integer order, including a complex order. Applications of fractional calculus theory in controller field have been proposed for OWES [12] in order to achieve a less harmonic content. The use of fractional-order PI^{μ} controllers can improve properties and controlling abilities over classical PI controllers.

Several approaches are possible for defining a fractional-order derivative and a fractional-order integral. The Caputo definition for the fractional-order derivative is given by:

$${}_a^C D_t^{\mu}\ f(t) = \frac{1}{\Gamma(n-\mu)} \int_a^t \frac{f^{(n)}(\tau)}{(t-\tau)^{\mu-n+1}}\, d\tau \tag{32}$$

where

$$\Gamma(x) \equiv \int_0^{\infty} y^{x-1}\, e^{-y}\, dy \tag{33}$$

while the Riemann–Liouville definition of fractional-order integral is given by:

$${}_a D_t^{-\mu}\ f(t) = \frac{1}{\Gamma(\mu)} \int_a^t (t-\tau)^{\mu-1} f(\tau)\, d\tau \tag{34}$$

$\Gamma(x)$ is the Euler's Gamma function, a and t are the limits of the integration, and μ identifies the fractional order.

In this article, μ is assumed as a real number that satisfies the restrictions $0 < \mu < 1$. Also, $a = 0$ and the following notational convention ${}_0 D_t^{-\mu} \equiv D_t^{-\mu}$ are assumed.

The fractional-order controller design is characterized in comparison with the classic one by having the additional advantage of augmenting the freedom for achieving an enhanced behavior [12], due to the advantage of having more criterion than the classical one, implied by the ability of weighting the past effects at each action of the controller. A fractional-order controller has a dynamical behavior described by a fractional differential integral equation with a derivative or an integral having at least a non-integer order.

5. CONTROL MODELING

A fractional-order PI^{μ} controller implement the controller strategy considered in the simulation for the variable-speed operation of the wind turbine with PMSG and a TLC. The

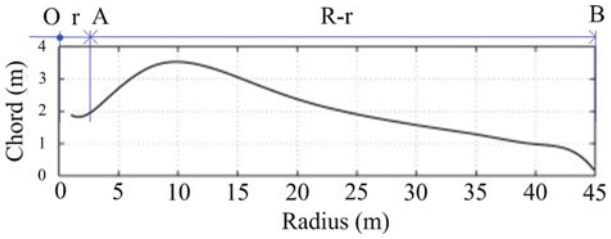

FIGURE 5. Blade radius r and R [31].

fractional-order PI^{μ} controller differential equation is given by:

$$f(t) = K_p\, e(t) + K_i\, D_t^{-\mu}\, e(t) \tag{35}$$

The fractional-order PI^{μ} has the advantage of being more flexible than the classical PI controller. This advantage is due to the existence of one more adjustable parameter, accounting for the intensity of integration.

Taking the order of integration μ equal to one in Eq. (35), a classical PI controller is obtained. The option [35] is followed for assessing the values of the parameters and circumvents the modeling of a mathematical programming problem, which is a different modeling. This type of option is the one normal in electric power systems to avoid a cumbersome modeling [36] for a fine tuning of parameters. The values of the parameters are given by a tradeoff compromised involving robustness and dynamics performance using tuning rules and favoring the range [0.4, 0.6] for the order of integration μ. The design of PI^{μ} controller follows the tuning rules in [35].

The control strategy of the OWES with a TLC using PI^{μ} controllers has the block diagram shown in Figure 6.

The wind speed and the marine wave are the most significant influence to the mechanical behavior of the OWES. Even a small variation in the wind speed may result in significant change in mechanical power, due to the cubic relationship between velocity and mechanical power Eq. (3). The rotor speed due to the mechanical inertia varies smoothly during the accumulation of the excess of energy as kinetic energy in the rotor and during the decrease. Smooth fluctuations in the rotor speed are expected, but a change on the value of the rotor speed occurs if an augmentation or a decrease happens in the stored kinetic energy [37, 38]. When the OWES is operating at nominal wind speed, if a wind sudden gust appears an increase in rotor speed is expected up to 10%. This is due to the fact that the pitch control response is not instantaneous. The part of the energy not stored as kinetic energy is converted into electrical energy through a PMSG. As wind speed varies the electrical energy converted from the PMSG has a variable frequency and, therefore, needs to be converted into the constant one of the electric grid. The PMSG currents $i_{\alpha\beta}$ are controlled by the difference between the PMSG speeds ω_e^* and ω_e through the pitch control. The triggering of the rectifier insulated gate bipolar transistors (IGBTs) is carried out using the difference $e_{\alpha\beta}$ between the PMSG currents $i_{\alpha\beta}$ and the rectifier controller current $i_{\alpha\beta}^*$ and also using the difference between the PMSG speeds ω_e^* and ω_e.

The difference between the electric grid voltage u_{dq} and the reference voltage u_{dq}^* is processed by the inverter PI^{μ} controller in order to determine a reference for the inverter currents. The triggering of the inverter transistors IGBTs is carried out using the difference between the electric grid current and the inverter controller reference current.

The convenient vector selection to ensure stability for the TLC after being processed by the hysteresis comparator in the block of SM control and SVM are given in [12]. The SM control is a lower level of control as is normally implemented with the PI^{μ} controller, for triggering the converters transistors is used PWM by SVM supplemented with SM. Physical constraints due to the power semiconductors have to be considered

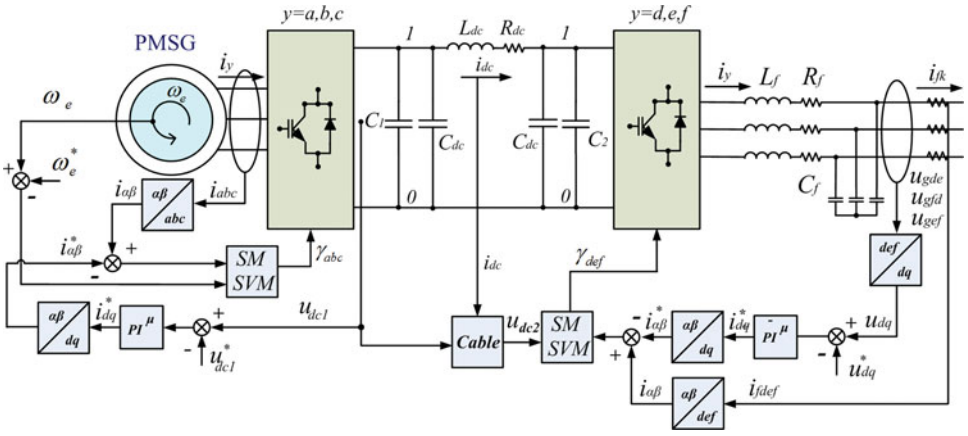

FIGURE 6. Diagram of an OWES with TLC employing PI^{μ} controllers.

during design phase and simulation studies. Particularly, the constraint of power semiconductors due to the fact of having a non-infinite switching frequency, implying that an error on the electric current between the reference value and the control value have to be tolerated. For instance, the finite value of switching frequency of 2, 5, or 10 kHz are normally reported.

Based on the Concordia ($\alpha - \beta$) transformation, in order to guarantee that the system follows the sliding surface $A(e_{\alpha\beta}, t)$, where $e_{\alpha\beta}$ is the error on the electric currents in the $\alpha\beta$-plane [33], is necessary that the error trajectory in the neighboring of the sliding surface observes the stability conditions given by:

$$A(e_{\alpha\beta}, t)\ \frac{dA(e_{\alpha\beta}, t)}{dt} < 0 \tag{36}$$

The sliding surface in current practice is chosen in way to allow a small error $\tau > 0$ for $A(e_{\alpha\beta}, t)$. This is due to power semiconductors switching finite frequency. But, for the simulation studies, an implementation of the switching strategy considered may be implemented by hysteresis comparators performing accordingly to the condition given by:

$$-\tau < A(e_{\alpha\beta}, t) < +\tau \tag{37}$$

This implementation of the switching strategy is implemented in the SM, SVM block, see Figure 7. The outputs of the hysteresis comparators are the integer variables $\delta_{\alpha\beta} = (\delta_\alpha,\ \delta_\beta)$ [33]. For the TLC, the output voltage vectors lie between level 0 and level 1, vector a_0 and h_0 are vectors for level 0 and vectors from b_1 through g_1 are vectors for level 1. The output voltage vectors in the $\alpha\,\beta$ plane are shown in Figure 7.

The integer voltage variables δ_α and δ_β are given by:

$$\delta_\alpha,\ \delta_\beta\ \in \{-1,\ \ 0,\ \ 1\} \tag{38}$$

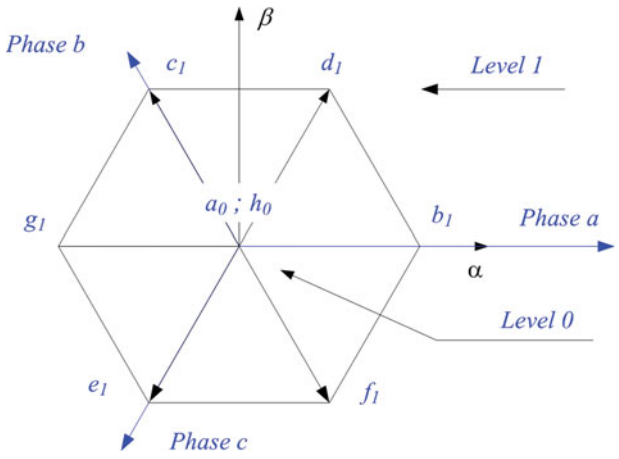

FIGURE 7. Output voltage vectors for the TLC.

$\delta_\beta \backslash \delta_\alpha$	–1	0	1
–1	e_1	e_1; f_1	f_1
0	g_1	a_0; h_0	b_1
1	c_1	c_1; d_1	d_1

TABLE 1. Generic output voltage vectors selection for the TLC, with the redundant inner vectors

Turbine moment of inertia	5500×10^3 kgm^2
Turbine rotor diameter	90 m
Hub height	80 m
Tip speed	17.64–81.04 m/s
Rotor speed	6.9–31.6 rpm
Generator rated power	2000 kW
Generator moment of inertia	400×10^3 kgm^2

TABLE 2. OWES data

For the TLC, the generic output voltage vector selection [33, 34] is shown in Table 1.

6. CASE STUDY

The wind speed for the operational range of the OWES is from 5 to 20 m/s and the switching frequency for transistors are 10 kHz. The mechanical eigenswings are given in [24]. The significant wave elevation and the frequency are 10 m and 0.25 Hz, respectively. The fractional controllers parameters are $\mu = 0.5$, $K_p = 50$, and $K_i = 2.6$ following [35]. A rated electric power of 2 MW is considered for the OWES, more data is in Table 2.

A wind speed upstream of the rotor given by a ramp increase is considered in the simulation taking 2.5 s between the speeds of 5 and 20 m/s. Also, a time horizon of 6 s is considered. The dynamics associated with the action excited by the wind on all physical structure is considered by a wind speed profile without perturbations or with perturbations.

The marine elevation is shown in Figure 8.

The flexible blade torque (blue), the rigid part of the blades plus hub torque (green) and the electric torque (red) for the three-mass model of the OWES, with and without wind perturbations are shown in Figure 9a and 9b.

For a wind without perturbations the flexible blade torque, the rigid part of the blades plus hub torque and the electric torque show a difference due to the kinetic energy to be stored in the respective masses, but after that, both torques converge to almost the same value, i.e., the dynamics enters on an almost stationary state. For a wind with perturbations the flexible blade torque is significantly perturbed by the wind, presenting an oscillatory behavior due to the perturbations associated with

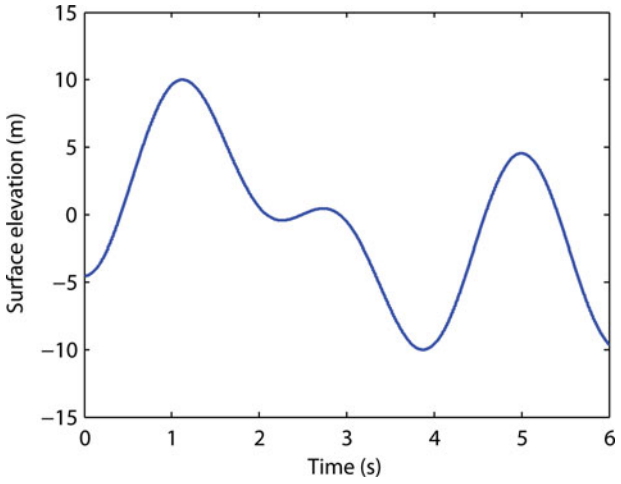

FIGURE 8. The marine elevation.

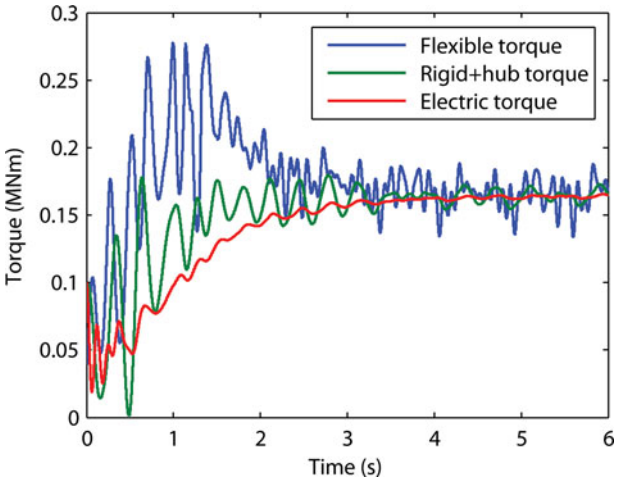

FIGURE 9b. Three-mass model: flexible blade torque, rigid blade plus hub torque, and electric torque: wind with perturbations.

the energy captured, which is a significant portion due to the relative lengths of the flexible blade part in comparison with the rigid one. The rigid part of the blades plus hub torque is also affected but with smaller intensity. The electric torque is almost the same as with a case of wind without perturbations, i.e., an identical behavior toward the stationary state is observed.

The rotor angular speed of the flexible blade (blue), the rotor angular speed of the rigid part of the blades plus hub (green) and the rotor angular speed of the generator (red), with and without wind perturbations are shown in Figure 10a and 10b.

For a wind without perturbations, the rotor angular speed of the flexible blade, the rotor angular speed of the rigid part of the blades plus hub, and the rotor angular speed of the generator show that the mass speeds have a convergence to a value identifying the stationary state. For a wind with perturbations the rotor angular speeds have a convergence to a value identifying the stationary state with added small oscillations in comparison with the wind without perturbations.

The submarine cable results for the reference voltage (blue) in what regard the continuous rectifier output (green) and the inverter input (red) voltages, with and without wind perturbations are shown in Figure 11a and 11b.

For a wind without perturbations Figure 11a shows that the reference voltage on the capacitor banks is attained with a satisfactory convergence in a few seconds. For wind with

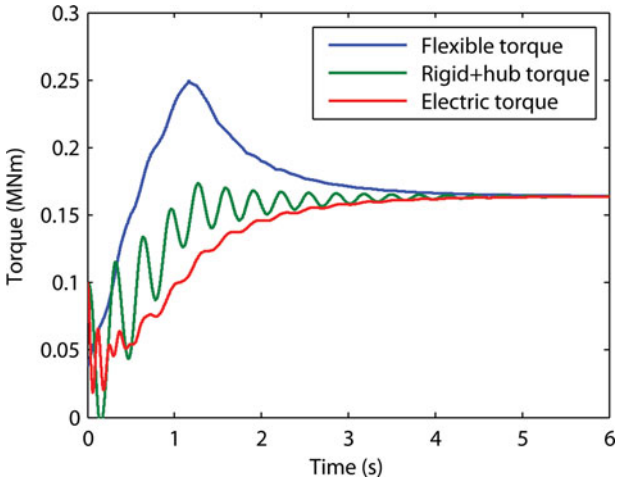

FIGURE 9a. Three-mass model: flexible blade torque, rigid blade plus hub torque, and electric torque: wind without perturbations.

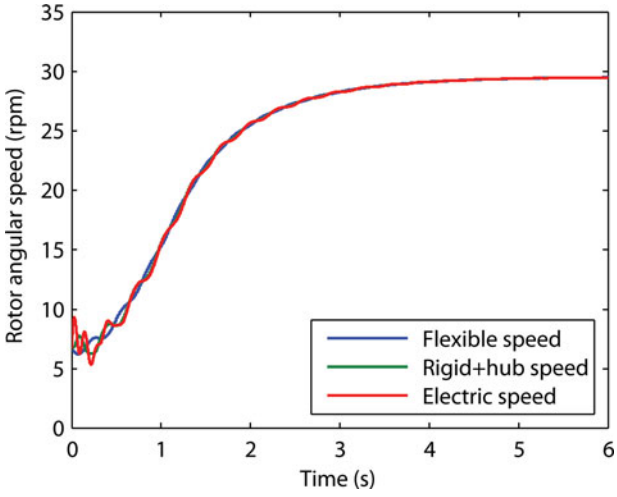

FIGURE 10a. Three-mass model: rotor angular speed of the flexible blade, rigid blade plus hub, and generator: wind without perturbations.

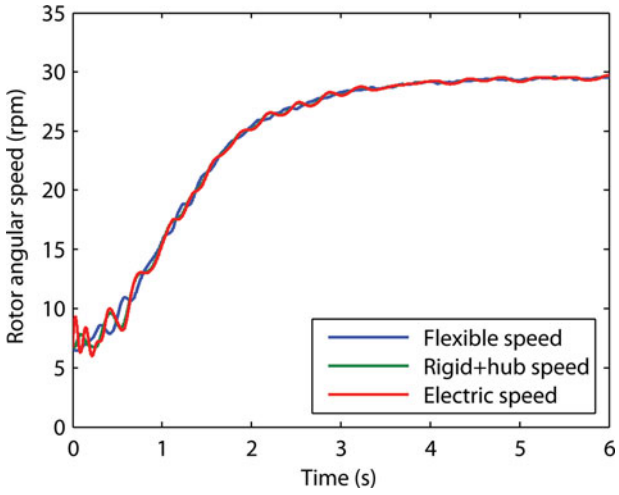

FIGURE 10b. Three-mass model: rotor angular speed of the flexible blade, rigid blade plus hub, and generator: wind with perturbations.

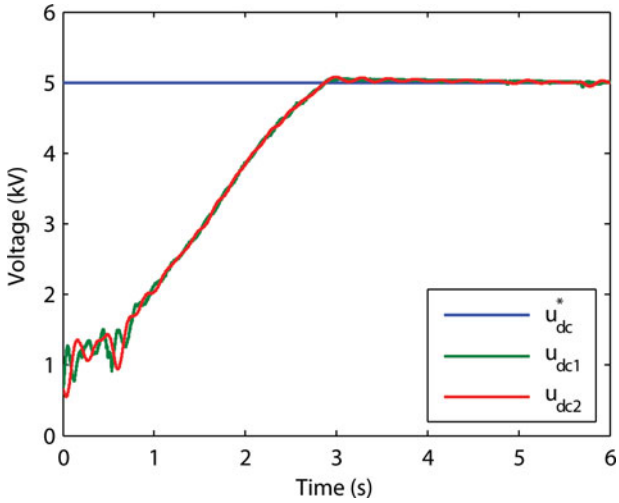

FIGURE 11b. Three-mass model: reference voltage, continuous rectifier output, and inverter input voltages for the submarine cable: wind with perturbations.

perturbations Figure 11b shows that the wind perturbations are attenuated and almost after a few seconds cease to have influence on the capacitor banks voltage, i.e., the reference voltage on the capacitor banks is attained with a satisfactory convergence.

The wind perturbations are not a cause of significant influence on the capacitor banks voltage, i.e., the voltage on the capacitor banks is almost immune to the perturbations as an implication of what is seen on the behavior of the electric torque.

The DC currents for the submarine cable for one-mass (blue), two-mass (green), and three-mass (red), with and without wind perturbations are shown in Figure 12a and in Figure 12b.

For a wind without perturbations Figure 12a shows that the DC current for the submarine cable presents an oscillatory behavior, with a more intense behavior for the three-mass model as expected due to the relevance of the added dynamics. For a wind with perturbations Figure 12b the DC currents have added small oscillations in comparison with the wind without perturbations.

The simulation of the OWES exposes the electromagnetic charge of the DC cable. The charge of the electric field of the cable occurs, first, as seen by the fact of the DC voltage, Figure 11, reaching almost the final reference voltage at three seconds,

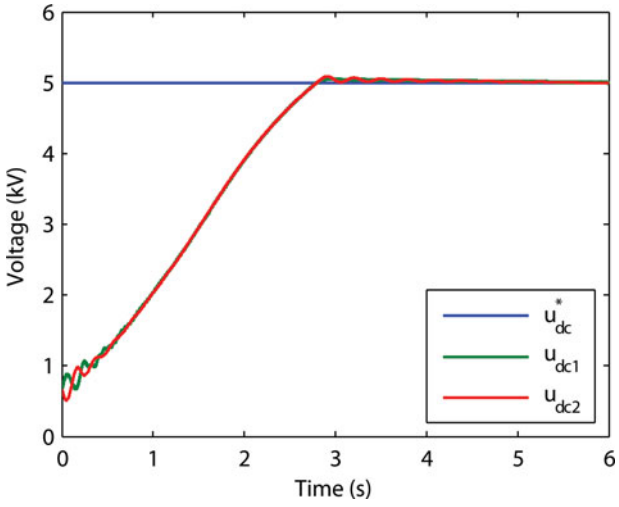

FIGURE 11a. Three-mass model: reference voltage, continuous rectifier output, and inverter input voltages for the submarine cable: wind without perturbations.

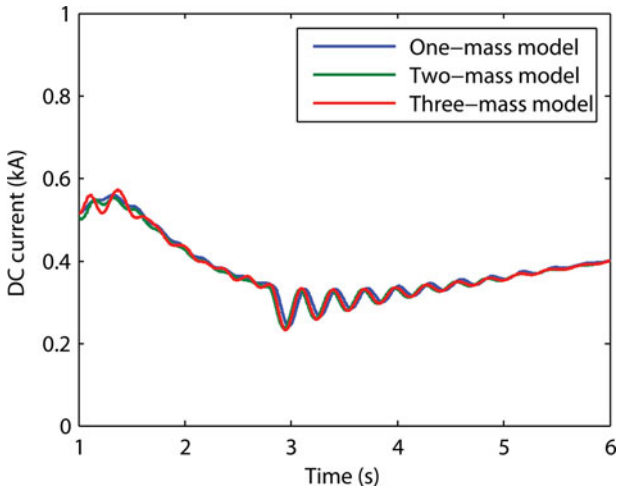

FIGURE 12a. One, two, and three-mass model: DC current for the submarine cable: wind without perturbations.

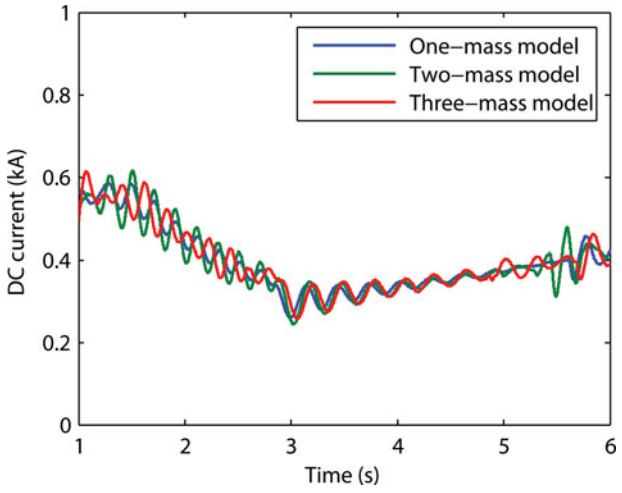

FIGURE 12b. One, two, and three-mass model: DC current for the submarine cable: wind with perturbations.

before the current, Figure 12, of cable stabilization. The current of the cable is associated with the charge of the magnetic field of the cable. This magnetic field charge is transient of the type of a transient on a series of an inductance with a resistance due to the model followed for the cable Figure 1, and has a high time constant than the electric one in this simulation.

The angular deviation of the flexible blade (blue), θ_{fbh}, the angular deviation of the rigid part of the blades plus hub (green), θ_{he}, for the three-mass model and the angular deviation of the generator (red), θ_{be}, for the two-mass model are shown in Figure 13.

Figure 13 shows an acceptable mechanical stress in the rotor in what regards the torsional effect, but the oscillations are better revealed with the three-mass modeling.

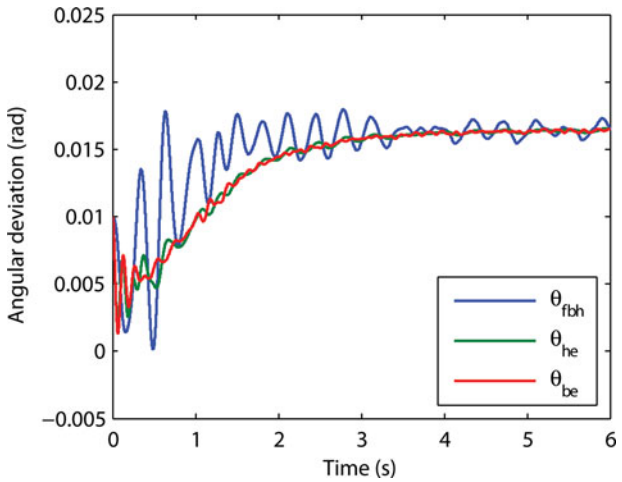

FIGURE 13. Wind with perturbations, two and three-mass model: angular deviation.

Output current	THD (%)		
	One-mass	Two-mass	Three-mass
Without perturbations	2.22	2.43	2.74
With perturbations	3.01	3.61	3.97

TABLE 3. THD of the current injected into the electric grid

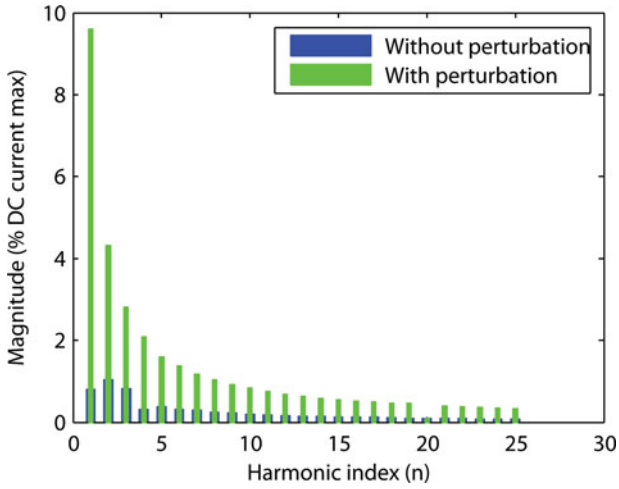

FIGURE 14. Wind with or without perturbations, three-mass model: DC current harmonic index for the submarine cable.

The average THD of the current injected in the electric grid for one-mass, two-mass, and three-mass models are shown in Table 3.

Table 3 shows that with the TLC, the THD of the output current is lower than the 5% limit imposed by IEEE-519 standard [40], for the three mass models. The three-mass model shows more sensitive due to the system dynamics over the one-mass and the two-mass models in what regards THD values. The comparison of results for the wind with or without perturbations is primarily asserted with the three-mass model to conclude about the interested in having a more sensitivity modeling.

The three-mass model results for the submarine cable DC current harmonic behavior without perturbations (blue) or with perturbations (green) are shown in Figure 14.

Figure 14 shows that the wind with perturbations introduces a harmonic behavior with larger component amplitudes while for the wind without perturbations components are almost negligible and is associated with the marine wave action.

7. CONCLUSIONS

The simulations are carried out for one, two, and three-mass drive train modeling to conclude on the THD associated with

the energy injected into the electric grid and make an evaluation of how the perturbations on the energy captured due to the wind and the marine waves are attenuated at the injection point. The THD obtained by the simulations is not in favor of a particularly modeling, but nevertheless the three-mass drive train modeling reveals a more accurate observation of the stress behavior in what regards the torques and the angular deviations subjected by the rotor. The simulations are in favor of the model for the OWES, revealing an adequate performance of the system.

FUNDING

This work is funded by Portuguese Funds through the Foundation for Science and Technology-FCT under the project LAETA 2015-2020, reference UID/EMS/50022/2013.

REFERENCES

[1] Dashwood, J., "*The Outlook for Energy: A View to 2040*," Melbourn: CEDA—Committee for Economic Development of Australia, pp. 45–52, 2012.

[2] Abdel-Akher, M., and Mahmoud, K., "Unbalanced distribution power-flow model and analysis of wind turbine generating systems," *Euro. Trans. Electr. Power*, Vol. 23, No. 5, pp. 689–700, July 2013.

[3] Quadrelli, R., and Peterson, S., "The energy–climate challenge: recent trends in CO_2 emissions from fuel combustion," *Energy Policy*, Vol. 35, No. 11, pp. 5938–5952, November 2007.

[4] Del Rio, P., and Tarancón, M. A., "Analysing the determinants of on-shore wind capacity additions in the EU: An econometric study," *Appl. Energy*, Vol. 95, pp. 12–21, July 2012.

[5] Wu, J., Wang, Z. X., and Wang, G. Q., "The key technologies and development of offshore wind farm in China," *Renew. Sust. Energy Rev.*, Vol. 34, pp. 453–462, June 2014.

[6] Guan, M., and Xu, Z., "A novel concept of offshore wind-power collection and transmission system based on cascaded converter topology," *Internat. Trans. Elect. Energy Syst.*, Vol. 24, No. 3, pp. 363–377, March 2014.

[7] Esteban, M., and Leary, D., "Current developments and future prospects of offshore wind and ocean energy," *Applied Energy*, Vol. 90, No. 1, pp. 128–136, February 2012.

[8] Lange, B., Larsen, S., Højstrup, J., and Barthelmie, R., "Importance of thermal effects and sea surface roughness for offshore wind resource assessment," *J. Wind Engineer. Indust. Aerodynamics*, Vol. 92, No. 11, pp. 959–988, September 2004.

[9] Luo, N., Bottasso, C. L., Karimi, H. R., and Zapateiro, M. "Semiactive control for floating offshore wind turbines subject to aero-hydro dynamic loads," *Proc. International Conference on Renewable Energies and Power Quality (ICREPQ'11)*, pp. 1–6, Las Palmas de Gran Canaria, Spain, April 2011.

[10] Tudorov, M., and Vukov, G., "Parametric torsional vibrations of a drive train in horizontal axis wind turbine," *Proc. 1ère Conférence Franco-Syrienne sur les Energies Renouvelables*, pp. 1–17, Damascus, Syria, October 2010.

[11] Xing, Z. X., Liang, L. Z., Guo, H. Y., and Wang, X. D., "Damping control study of the drive train of DFIG wind turbine," *Proc. Int. Conf. on Energy and Environment Technology*, pp. 576-579, Guilin, China, October 2009.

[12] Seixas, M., Melicio, R., and Mendes, V. M. F., "Fifth harmonic and sag impact on PMSG wind turbines with a balancing new strategy for capacitor voltages," *Energy Conver. Management*, Vol. 74, pp. 721–730, March 2014.

[13] Pican, E., Omerdic, E., Toal, D., and Leahy, M., "Direct interconnection of offshore electricity generators," *Energy*, Vol. 36, No. 3, pp. 1543–1553, March 2011.

[14] Dicorato, M., Forte, G., and Trovato, M., "Wind farm stability analysis in the presence of variable-speed generators," *Energy*, Vol. 39, No. 1, pp. 40–47, March 2012.

[15] Negra, N. B., Todorovic, J., and Ackermann, T., "Loss evaluation of HVAC and HVDC transmission solutions for large offshore wind farms," *Elect. Power Syst. Res.*, Vol. 76, No. 11, pp. 916–927, July 2006.

[16] Shao, S. J., and Agelidis, V. G., "Review of DC system technologies for large scale integration of wind energy systems with electricity grids," *Energies*, Vol. 3, pp. 1303–1319, June 2010.

[17] Srivastava, S., "Analysis of HVDC and HVDC light technology," *Advance Elect. Elec. Engin.*, Vol. 3, No. 6, pp. 711–716, June 2013.

[18] Seixas, M., Melicio, R., and Mendes, V. M. F., "Simulation of rectifier voltage malfunction on OWECS, four-level converter, HVDC light link: Smart grid context tool," *Energy Conver. Manag.*, Vol. 97, pp. 140–153, June 2015.

[19] Hammons, T. J., "Power cables in the twenty-first century," *Elec. Power Comp. Sys.*, Vol. 31, No. 10, pp. 967–994, June 2010.

[20] Agelidis, V. G., Demetriades, G. D., and Flourentzou, N., "Recent advances in high-voltage direct-current power transmission systems," *Proc. IEEE International Conference on Industrial Technology*," pp. 206–213, Mumbai, India, December 2006.

[21] Balogh, E., "Deepwater offshore wind power generation using oil and gas platform technology," 2008, available at http://www.renewableenergyworld.com/rea/news/article/2008/12/deepwater-offshore-wind-power-generation-using-oil-and-gas-platform-technology-54314

[22] Belenguer, E., Vidal, R., Blasco-Giménez, R., Beltran, H., Alfonso, J. C., and Ariño, C., "Islanded operation and control of offshore wind farms connected through a VSC-HVDC link," *Proc. International Conference on Renewable Energies and Power Quality*, pp. 1–6, Bilbao, Spain, March 2013.

[23] Aktarujjaman, M., Kashem, M. A., Negnevitsky, M., and Ledwich, G., "Black start with DEIG based distributed generation after major emergencies," *Proc. IEEE Power Electronics, Drives and Energy Systems for Industrial Growth*, pp. 1–6, New Delhi, India, December 2006.

[24] Akhmatov, V., Knudsen, H., and Nielsen, A. H., "Advanced simulation of windmills in the electric power supply," *Internat. J. Elect. Power Energy Syst.*, Vol. 22, No. 6, pp. 421–434, August 2000.

[25] Slootweg, J. G., Polinder, H., and Kling, W. L., "Representing wind turbine electrical generating systems in fundamental frequency simulations," *IEEE Transactions Power Systems*, Vol. 18, No. 4, pp. 516–524, December 2003.

[26] Eikeland, F. N., *Compensation of Wave-Induced Motion for Marine Crane Operations*, Master Thesis, Norwegian University of Science, Norway, 2008.
[27] Seixas, M., Melício, R., and Mendes, V. M. F., "Simulation of offshore wind turbine link to the electric grid through a four-level converter," in *Proc. 5th DoCEIS 2014 Technological Innovation Collective Awareness Systems*, L. M. Camarinha-Matos, N. S. Barrento, and R. Mendonça (Eds.), Heidelberg: Springer, pp. 324–331, 2014.
[28] Holierhoek, J., "Investigation into the possibility of flap-lag-stall flutter," *Proc. 45th AIAA Aerospace Sciences Meeting and Exhibit*, pp. 1–12, Reno, NV, January 2007.
[29] Chaviaropoulos, P. K., "Flap/lead-lag aeroelastic stability of wind turbine blade sections," *Wind Energy*, Vol. 2, No. 2, pp. 99–112, April/June 1999.
[30] Ramtharan, G., and Jenkins, N., "Influence of rotor structural dynamics representations on the electrical transient performance of DFIG wind turbines," *Wind Energy*, Vol. 10, No. 4, pp. 293–301, July/August 2007.
[31] Buckney, N., Pirrera, A., Green, S. D., and Weaver, P. M., "Structural efficiency of a wind turbine blade," *Thin-Walled Structures*, Vol. 67, pp. 144–154, June 2013.
[32] Manwell, J. F., McGowan, J. G., and Rogers, A. L., *Wind Energy Explained: Theory, Design and Application, 2nd ed*., West Sussex: Wiley, pp. 83–105, December 2009.
[33] Senjyu, T., Tamaki, S., Urasaki, N., and Uezato, K., "Wind velocity and position sensorless operation for PMSG wind generator," *Proc. 5th Int. Conf. Power Electronics and Drive Syst.*, pp. 787–792, Singapore City, Singapore, November 2003.
[34] Seixas, M., Melicio, R., Mendes, V. M. F., and Pousinho, H. M. I., "Simulation of offshore wind system with two-level converters: HVDC power transmission," *Proc. 16th International Power Electronics and Motion Control Conference and Exposition*, pp. 1384–1389, Antalya, Turkey, 2014.
[35] Melício, R., Mendes, V. M. F., and Catalão, J. P. S., "A pitch control malfunction analysis for wind turbines with permanent magnet synchronous generator and full-power converters: proportional integral versus fractional-order controllers," *Elec. Power Comp. Syst.*, Vol. 38, No. 4, pp. 387–406, February 2010.
[36] Maione, G., and Lino, P., "New tuning rules for fractional PI-alfa controllers," *Nonlinear Dynamics*, Vol. 49, No. 1–2, pp. 251–257, July 2007.
[37] Muyeen, S. M., Al-Durra, A., and Tamura, J., "Variable speed wind turbine generator system with current controlled voltage source inverter," *Energy Convers. Manag.*, Vol. 52, No. 7, pp. 2688–2694, July 2011.
[38] Melicio, R., Mendes, V. M. F., and Catalão, J. P. S., "Power converter topologies for wind energy conversion systems: integrated modeling, control strategy and performance simulation." *Renewable Energy*, Vol. 35, No. 10, pp. 2165–2174, October 2010.
[39] Melicio, R., Mendes, V. M. F., and Catalão, J. P. S., "Wind turbines equipped with fractional-order controllers: stress on the mechanical drive train due to a converter control malfunction." *Wind Energy*, Vol. 14, No. 1, pp. 13–25, January 2011.
[40] IEEE Guide for Harmonic Control and Reactive Compensation of Static Power Converters. IEEE Standard 519–1992, 1992.

BIOGRAPHIES

Mafalda Seixas is a researcher at the Center of Intelligent Systems, IDMEC, Instituto Superior Técnico (IST), Universidade de Lisboa and an Adjunct Professor at Instituto Superior de Engenharia de Lisboa (ISEL), Portugal. She received her Ph.D. from Universidade de Évora, Portugal, in 2015 in mechatronics and energy engineering. She is currently a Post Ph.D. student. She has authored or co-authored peer-reviewed articles presented at book chapters, international conferences, or published in journals. Her areas of research interests are renewable energy, particular wind energy; power electronics.

Rui Melício is a researcher at the Center of Intelligent Systems, IDMEC, Instituto Superior Técnico (IST), Universidade de Lisboa and an Assistant Professor with Habilitation at Universidade de Évora (UE), Portugal. He received his MSc IST, in 2004, his Ph.D. from the Universidade da Beira Interior, in 2010, the Post-Ph.D. Science of the Portuguese Foundation, in 2012, all in electrical engineering, the habilitation in mechatronics and energy engineering UE, in 2014. He has worked more the 20 years in the electrical and oil industries. He has supervised Post-Ph.D., Ph.D., and M.Sc. students. He has participated in national and international projects. He has authored or co-authored patents, peer-reviewed articles presented at book chapters, international conferences, or published in journals, prototypes, and technical reports. He is a Senior Member of the IEEE Industrial Electronics Society. His areas of research interest are power systems management and operation, renewable energy, particular wind and solar energy, and power electronics.

Victor Mendes is a Coordinate Professor at Instituto Superior de Engenharia de Lisboa (ISEL), Portugal, at the Energy and System Division, invited Full Professor at the Universidade de Évora (UE), and researcher at the CAST—Centre for Aerospace Science and Technology, member of the panel for Electronic, Electrical Engineering, and Computer Science of the Portuguese Foundation for Science and Technology (FCT) for evaluation of doctoral and post-doctoral scholarships. He holds the academic title of Habilitation in Electrotechnical Engineering from Universidade da Beira Interior; his PhD and M.Sc in Electrical Engineering and Computer Science, the Graduation degree in Electrical Engineering, Power Systems, from Instituto Superior Técnico (IST), Universidade de Lisboa. His areas of research interests are mathematical programming, power systems management and operation; renewable energy, particular wind and solar energy; power electronics, electric market support managing systems.